RSC Advances

ROYAL SOCIETY OF CHEMISTRY

www.rsc.org/advances

Sheet-like structure FeF_3/graphene composite as novel cathode material for Na ion batteries

Yongqiang Shen [ab], Xianyou Wang*[a], Hai Hu [a], Miaoling Jiang [a], Yansong Bai [a], Xiukang Yang [a], Hongbo Shu [a]

([a] *Key Laboratory of Environmentally Friendly Chemistry and Applications of Ministry of Education，Hunan Province Key Laboratory of Electrochemical Energy Storage and Conversion，School of Chemistry, Xiangtan University, Hunan, Xiangtan 411105, China;*

[b] *College of Chemistry and Chemical Engineering, Jishou University, Jishou 416000, China*)

Abstract: A sheet-like structure FeF_3/graphene composite is successfully synthesized by a novel and facile sol-gel method. The structure and electrochemical performance of the as-synthesized FeF_3/graphene composite are investigated by X-ray diffraction (XRD), scanning electron microscope (SEM), transmission electron microscopy (TEM), high-resolution TEM (HRTEM) and electrochemical measurement. The results indicate that the FeF_3 nanosheets are loaded on the surface of the graphene sheets to form the sheet-like structure hybrid. Fourier transform infrared (FTIR) spectrum confirms that C-F bonds exist in FeF_3/graphene composite, and it further indicates that a chemical bond between FeF_3 and graphene has been formed and FeF_3 can preferably stick to the surface of the graphene. The FeF_3/graphene composite as cathode material of rechargeable Na ion batteries (NIB) exhibits a fairly high initial discharge capacity of 550 mAh g^{-1} at 0.1 C, and it still keeps a capacity of 115 mAh g^{-1} after 50 cycles at 0.3 C at a range of 1.0-4.0 V for NIB.

* **Corresponding author:** Xianyou Wang, Tel: +86 731 58292060; Fax: +86 731 58292061.
E-mail address: wxianyou@yahoo.com (X. Wang).

Keywords: Na ion batteries; Iron fluorides; Graphene; Sheet-like structure; Sol-gel method

1. Introduction

For the past decade, Li ion batteries (LIB) have been extensively used in the consumer electronics, military, electric vehicle and aerospace fields due to their excellent energy density, good power capability, and long cycle life. However, along with the development of low cost and high efficient recycling technology, the low abundance of lithium in the earth's crust and large-scale applications of LIB become controversial. Alternatively to the widely studied LIB, the NIB can be a suitable choice for smart grid, energy conversion and storage applications in terms of the low cost, safety and natural abundance of sodium resources [1]. For the past decade, many efforts have been devoted to the development of novel cathode active materials. Transition metal oxide compounds and polyanion compounds with layered structure have been investigated as the cathode materials for NIB, such as $Na_{0.44}MnO_2$ [2-3], $Na_4Mn_9O_{18}$ [4], $Na_{0.71}CoO_2$ [5], $NaNi_{1/3}Mn_{1/3}Co_{1/3}O_2$ [6], $Na[Ni_{1/3}Fe_{1/3}Mn_{1/3}]O_2$ [7], $Na_{2/3}Ni_{1/3}Mn_{2/3-x}Ti_xO_2$ [8], $Na_2FeP_2O_7$ [9], $Na_2CoP_2O_7$ [10], $Na[Fe,Mn]PO_4$ [11], $Na_3V_2(PO_4)_3$ [12], $Na[Mn_{1-x}M_x]PO_4$ (M = Fe, Ca, Mg) [13]. Recently, transition metal fluorides have been considered as a promising new class of cathode materials for LIB, which exhibit large theoretical capacities and high discharge voltages due to their highly ionic metal-ligand bonds and small atomic weight. Unlike conventional intercalation reaction, transition metal fluorides, based on reversible conversion

reaction, enable the full utilization of redox during the charge/discharge process and thus possess high theoretical specific capacity. Especially, due to high theoretical capacity and theoretical energy density, FeF_3 have been researched as new and promising cathode materials for LIB [14-17, 18-20]. Besides, iron based fluorides have attracted interest as a promising positive electrode for rechargeable Na batteries. The important fluoride materials are currently reported as Na-ion batteries cathodes, such as FeF_3 [14-17] and $NaFeF_3$ [21, 22]. Li and his coworkers reported $FeF_3 \cdot 0.33H_2O$ and $FeF_3 \cdot 0.5H_2O$ wired by carbon nanotubes through ionic-liquid-based synthesis method for Na-storage, and which exhibited a considerable capacity and rate performances as cathode materials for NIB [15, 16]. Because of the dense structure and high insulating character of pure FeF_3, the electrochemical performance deteriorates promptly as the cathode material of LIB, let alone NIB [15].

Usually, FeF_3 used as cathode materials of LIB or NIB is its hydrated compounds. Besides, it has also been reported that lithium aluminate nanosheet and α-Fe_2O_3 nanoplates well-dispersed on the graphene can enhance their ionic conductivity [23, 24]. In order to overcome the intrinsic drawback of the FeF_3, a sheet-like structure FeF_3 loaded by graphene is first designed and synthesized via a novel and facile sol-gel route in this work. The FeF_3/graphene nanosheets are obtained by controlling the dry temperature and the amount of graphene in a bottom-up synthesis. Herein, graphene is both used as the conductive agent to further improve the electrical conductivity of FeF_3 and a supporter for the stabilization of iron fluoride nanosheets.

The FeF_3 nanosheets and graphene stack each other to form a hierarchical electron/ion conducting network, arising from the bilateral interaction of iron fluoride nanosheets and graphene sheet. The morphology and electrochemical performances of the sheet-like FeF_3/graphene composites are subsequently investigated as cathode material for NIB.

2. Experimental

$Fe(NO_3)_3 \cdot 9H_2O$ (10 mmol, 4.04 g) and conduction type graphene 0.1 g (8% of total weight) (The Sixth Element Inc) were dissolved or suspended in 50 mL methanol, then 1.5 ml (30 mmol) of 40% HF acid was added with stirring to gain a solution. The obtained $FeF_3 \cdot 3H2O$ sol was aged for 24 h before dried at 60 °C. The product xerogel was further dried at 180 °C for 8h in a vacuum drying oven and ground into fine powders.

X-ray powder diffraction was performed using Rigaku D/MAX-2500/PC equipped with Cu-Ka source (40 kV, 250 mA) to get the crystal structure. The sizes and morphologies of compound particles were characterized by a field emission scanning electron microscope using JEOL JSM-3500N. Transmission electron microscopy (TEM), selected area electron diffraction (SAED) and high-resolution TEM (HRTEM) images were taken on a JEOL-2100 microscope instrument at an acceleration voltage of 200 kV.

The electrochemical performance of the as-synthesized material was characterized on 2025 type coin cells as a cathode and a sodium disk as anode for

Na-ion batteries. The cathodes for Na cells were fabricated by mixing the cathode material, Super carbon (SP), and polyvinylidene fluoride (PVDF) binder with a weight ratio of 80:15:5 in N-methyl pyrrolidinone, which were then pasted on aluminum foil followed by drying under vacuum at 110 °C for 24 h. The average mass loading of materials on aluminum foil is about 1.83 mg/cm^2. The test Na cells were assembled with the cathodes thus fabricated, metallic sodium anode, Glass fiber (GF/D) from Whatman was employed as the separator, and the electrolyte was 1 mol L^{-1} $NaClO_4$ in a solvent of propylene carbonate (PC). The assembly of the testing cells was carried out in an argon-filled glove box, where water and oxygen concentration were kept less than 5 ppm. The charge-discharge experiments were conducted on a battery cycler (Newell Battery Test) at 25 °C. Charge−discharge measurements of fluoride-based cathodes versus Na/Na^+ were performed at room temperature under various rates of 0.1−5 C in a voltage range of 1.2−4.0 V and 1.0−4.0 V for Na-storage. All of the specific capacities were calculated based on the mass of as-synthesized material (including graphene). Specifically, 0.1 C represents 23.7 mA g^{-1}, 0.3 C represents 71.1 mA g^{-1}, 1 C represents 237 mA g^{-1} and so on.

The galvanostatic intermittent titration technique (GITT) was performed at room temperature at a voltage range of 1.0-4.0 V. The GITT measurements were performed on the second cycle to determine the diffusion coefficient of Na ions (D_{Na}) in electrode active materials. To achieve nearly equilibrium state (Es), relaxing 60 min after an interval of 10 min at a current density of 0.1 C have been combined with the GITT test. The procedure continued until the cutoff voltage was reached. As shown in

Fig. S4, the Na ion diffusion coefficient can also be determined by GITT by Fick's second laws of diffusion and calculated according to the following equation:

$$D_{Na} = \frac{4}{\pi}\left(I_0 \frac{Vm}{FS} \right)^2 \left(\frac{dE/dx}{dE/dt^{1/2}} \right)^2$$

Where I_0 (A) is the applied current in the charge/discharge process, V_m (cm^3 mol^{-1}) is the molar volume of active materials, F (96485 C/mol) is the Faraday constant, S (cm^2) is the total contact area between the electrolyte and electrodes and L (cm) is the thickness of the electrode.

3. Results and discussion

Fig. 1a illustrates FeF_3 nanosheets anchored on the surface of graphene sheet to form the FeF_3/graphene composite with sheet-like structure. As schematically shown in Fig. 1a, firstly, $FeF_3 \cdot 3H_2O$, which is quickly formed after $Fe(NO_3)_3 \cdot 9H_2O$ and HF added in methanol solution, generates C-F bond with graphene for nucleation sites to induce surface nucleation of iron fluoride during the aged process. The new produced C-F bonds are expected to act as nucleation sites for $FeF_3 \cdot 3H_2O$ due to intermolecular interactions. Besides, controlling the graphene amount, the graphene sheets, which can anchor $FeF_3 \cdot 3H_2O$ crystal, can provide more growing spots for $FeF_3 \cdot 3H_2O$ crystals and can also prevent the growth of big fluoride nanocrystals, thus $FeF_3 \cdot 3H_2O$ nanocrystals distribute homogeneously on the surface of the graphene sheet, a $FeF_3 \cdot 3H_2O$/graphene composite precursor is obtained. Finally, the precursor was heated in a vacuum drying oven at the temperature of 180 °C to remove H_2O molecules and the sheet-like FeF_3/graphene composite was obtained.

From the SEM images in Fig. 1b, the FeF_3/graphene composite is actually the hierarchical sheet-like structure. A rough wavy structure could originate from the intrinsic wrinkles and ripples of graphene. The TEM images (Fig. 1(c, d)) confirm further that the FeF_3 nanosheets (red arrows) anchor on the surface of the graphene sheet (blue arrows) and form the hybrid with both sheet-like structure. The sizes of the nanosheets FeF_3/graphene range from several hundred nanometers to a few micrometers. As being seen from the inset of Fig. 1c, the SAED pattern shows a set of broad diffuse rings instead of spots due to the random orientation of the crystallites, corresponding to diffraction from different planes of the nanocrystallites, which indicate the FeF_3 nanosheets are formed by tiny the FeF_3 nanocrystallites instead of growing along a certain direction. The SAED patterns are consistent with a hexagonal phase structure of FeF_3 with strong ring patterns due to (012) and (024) planes. Moreover, it can also be found from Fig. 1d that the FeF_3 nanosheets are formed by self-assembly of numerous nanoparticles with various sizes from 10 nm to 100 nm, which stretch outwards from the aggregate core, thus presenting the nanosheets morphology. HRTEM image (Fig. 1e) also reveals that FeF_3 tiny nanocrystals were formed. Lattice fringes can be discerned from the HRTEM image, suggesting that the FeF_3 nanoparticles are well-crystallized. Fig. 1(e) show that the interplanar spacing is about 0.381 nm and 0.265 nm, which also corresponds to the distance of (012) and (104) planes of FeF_3, respectively, indicating that the nanoparticles are the iron based fluoride.

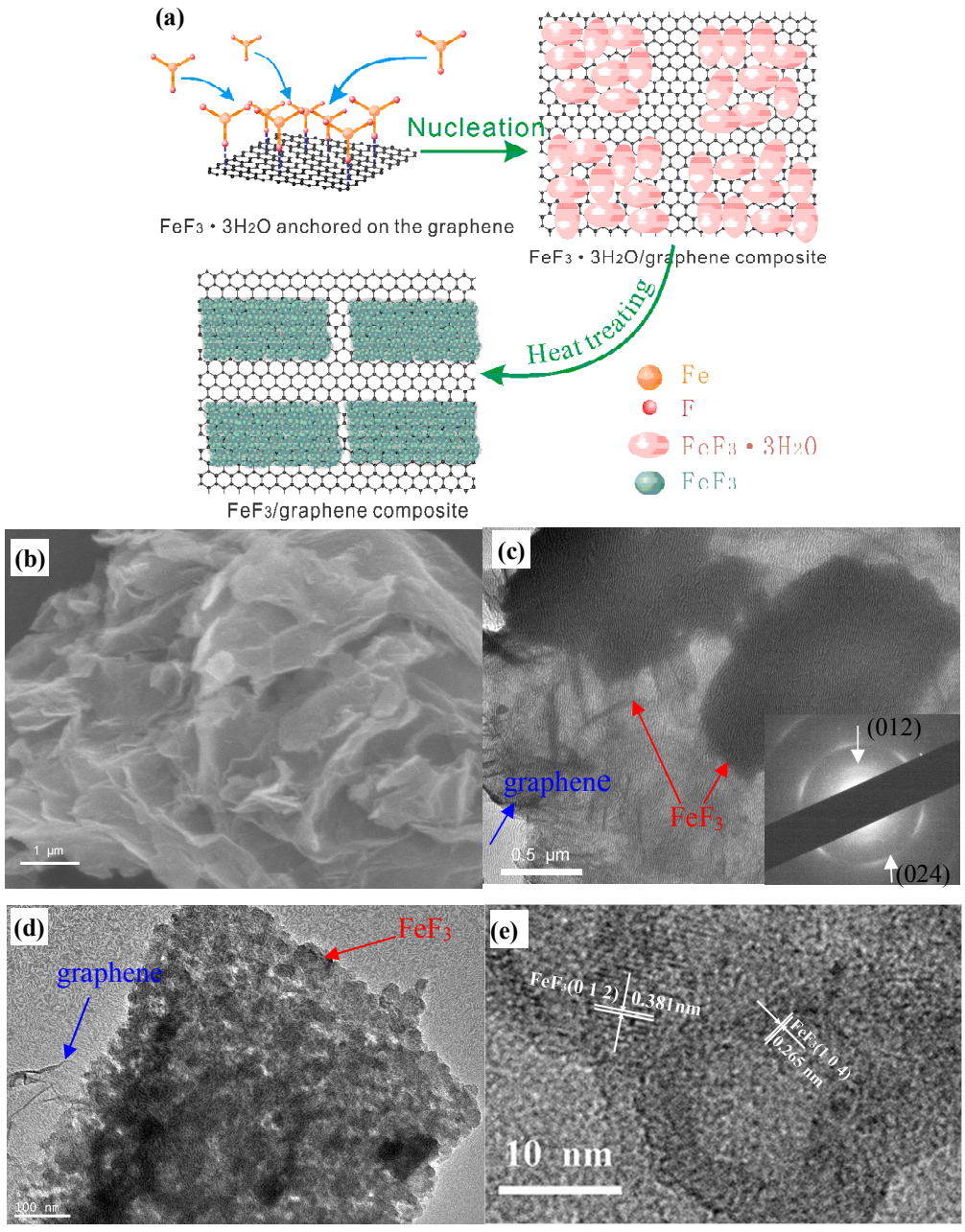

Fig. 1 (a) schematic illustration of fluoride nanosheet with graphene to form FeF_3/graphene, (b) SEM image, (c, d) TEM images, SAED image (the inset of (c)), and (e) HRTEM images of nanosheets FeF_3/graphene.

Fig. 2a, 2b and 2c represent the typical XRD patterns of the $FeF_3 \cdot 3H_2O$ precursor, graphene, and the synthesized FeF_3/graphene by sol-gel method, respectively. According to the Scherer formula: $D=R\lambda/(\beta\cos\theta)$, when 2θ is 15.940º, 22.641º and

25.580º in XRD pattern of $FeF_3 \cdot 3H_2O$ precursor, it can be calculated that the average particle sizes are 53.8 nm, 46 nm and 44.8 nm, respectively. The results indicate that the precursor consists of nanosized partticles. The peak locations in Fig. 2c indicate the formation of FeF_3/graphene composite. Moreover, a very small intensity reflection of graphene in Fig. 2c due to the presence of graphene can also be observed for the FeF_3/graphene composite. The broad reflections indicate its low crystallisation degree, which is one common feature shared by many nanoscopic metal fluorides [25]. In order to analyze the interaction of FeF_3 nanosheets with graphene sheets, Fourier transform infrared (FTIR) spectrum was used. The samples prepared as KBr pellets were recorded on a Perkin-Elmer Spectrum One FTIR spectrophotometer in a scan range of 400-4000 cm^{-1}, and the results are shown in Fig. 2d. The characteristic peak at approximately 530 cm^{-1} is an associated with the typical vibration band of Fe-F bond of FeF_3. Meanwhile, the C-F stretching vibrations are generally found at around 1070 cm^{-1}[17], which confirms that FeF_3 nanosheets tightly anchor on the surface of graphene sheets (as Fig. 1a) due to interaction of F atom with C atom each other, then the FeF_3/graphene composite with hybrid sheet-structure is formed.

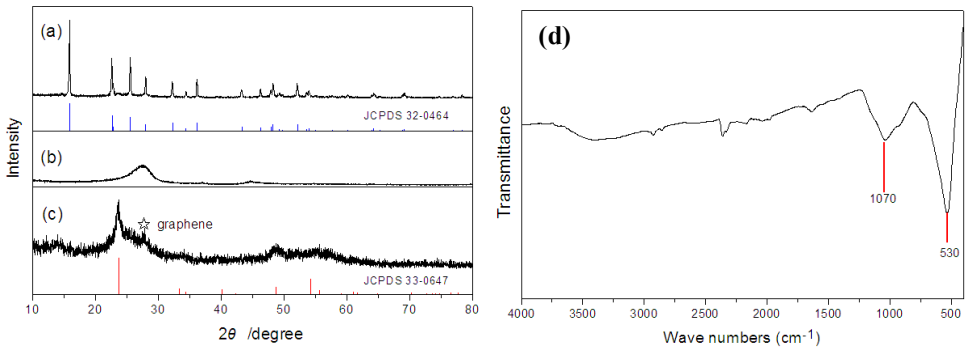

Fig. 2 XRD patterns of (a) the $FeF_3 \cdot 3H_2O$ precursor, (b) graphene and (c) FeF_3/graphene, (d) IR

spectra of nanosheets FeF_3/graphene.

Fig. 3a indicates the comparison of the rate capability for the FeF_3/graphene composite at a range of 1.0-4.0 V. The FeF_3/graphene cathode presents apparently a high irreversible discharge capacity of 550 mAh g^{-1} at the first cycle at 0.1 C. The discharge capacity is close to the theoretical capacity of FeF_3. It can also find from Fig. 3a that there is two reduction peaks at about 2.6 V and 1.2 V, which can correspond to the insertion/deinsertion reaction and the reversible conversion reaction, respectively. Usually, the electrode reaction mechanism of FeF_3 as the cathode material of Na ion battery can be expressed as following [26]:

$$FeF_3 + Na \rightarrow NaFeF_3 \ (4.0\sim1.2\ V) \quad (1)$$

$$NaFeF_3 + 2Na \rightarrow Fe + 3NaF \ (1.2\sim1.0\ V) \quad (2)$$

Equ.1 corresponds to the Na ion intercalation/unintercalation reactions between phases containing Fe^{3+} and Fe^{2+}. Equ.2 should be attributed to the redox reactions between phases containing Fe^{2+} and metallic Fe^0 based on chemical conversion mechanism. It can be found from Fig. 3b that although the first discharge capacity is high, the second discharge capacity drops down to 396 mAh g^{-1} and charge capacity dives to 388 mAh g^{-1}. The reasons of the sudden descent of capacity are likely to originate from not only the formation of insulating phases during conversion reaction but also the formation of solid electrolyte interphase (SEI) layers. The presence of a relatively stable conversion reaction for the FeF_3/graphene composite provides extra capacity for the first few cycles. However, the Fe^0 originated from Equ.2 will probably aggregate to form big particles during the charge/discharge cycle process,

thus it will result in the slow kinetics of the conversion reaction and the electrode process exhibits mainly the Na^+ insertion reaction after the 50th cycle. Besides, GITT test results in Fig. 3d and 3e show that the Na ion (D_{Na}) diffusion coefficient during insertion reaction is higher than during conversion reaction. Fig. 3c indicates the rate performance at different rates at the range of 1.5-4.0 V, in this potential window the electrode reaction only behaves the insertion/deinsertion reaction. To our surprise, the nanosheet FeF_3/graphene composite delivers 234 mAh g^{-1} in the insertion process at the first cycle at 0.1 C, which is nearly accordance with the theoretical capacity of 1 Na insertion. This high capacity is maybe ascribed to the special sheet-like structure of the FeF_3/graphene composite. Especially, the FeF_3/graphene electrode can deliver 90 mAh g^{-1} at 1 C rate at the range of 1.0-4.0 V (Fig. 3b), while it can only deliver about 60 mAh g^{-1} at the same rate at the range of 1.5-4.0 V (Fig. 3c). Compared Fig. 3b with Fig.3c, it can be found that the capacity provide by the insertion reaction is about two-thirds of the total capacity. Therefore, the sheet-like structure of FeF_3/graphene composite plays likely an important role for improving its capacity.

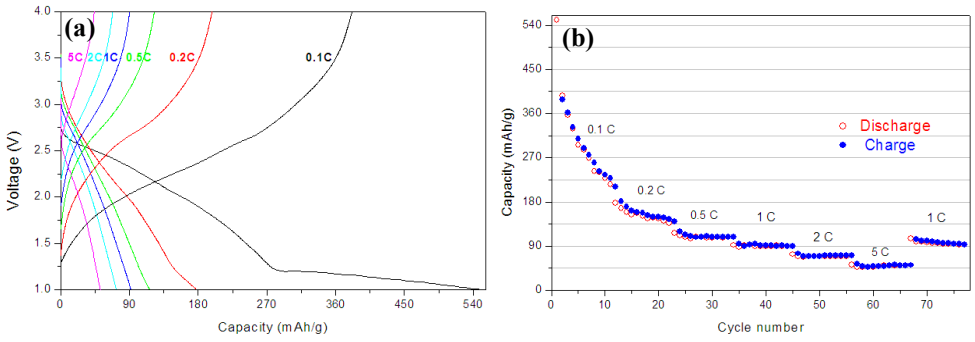

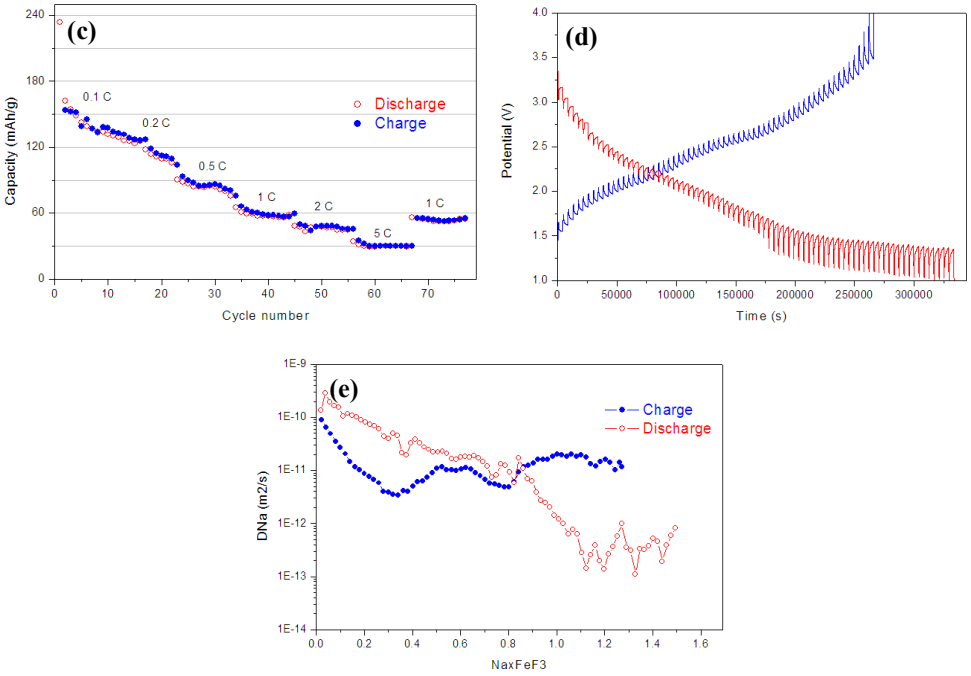

Fig. 3 electrochemical behavior for FeF_3/graphene: (a) Prolonged cycling behavior at different C rates, respectively at the range of 1.0-4.0 V, (b) rate performance at different rates at the range of 1.0-4.0 V, (c) rate performance at different rates at the range of 1.5-4.0 V, (d) the discharge/charge GITT curves of FeF_3/graphene electrode as a function of time in the potential range of 1.0-4.0 V, and (e) calculated D_{Na} for FeF_3/graphene as a function of *x* (the total Na insertion and conversion number) during charge/discharge process, respectively.

Fig. 4 shows the cycling performances of FeF_3/graphene and FeF_3 as the cathode material of NIB at 0.3 C at a range of 1.0-4.0 V. The capacities of FeF_3 and FeF_3/graphene composite during the first discharge are 91 and 344 mAh g^{-1}, respectively. The capacities of discharge decay faster in the first few cycles, but capacities during the later cycles decline slowly, and the discharge capacity of the FeF_3/graphene composite can still keep 115.8 mAh g^{-1} after 50 cycles. However, for the FeF_3 electrode the discharge capacity is only 10 mAh g^{-1} after the 50th cycle.

Apparently, the addition of graphene and formation of sheet-like structure between FeF_3 and graphene can well improve the electrochemical performance.

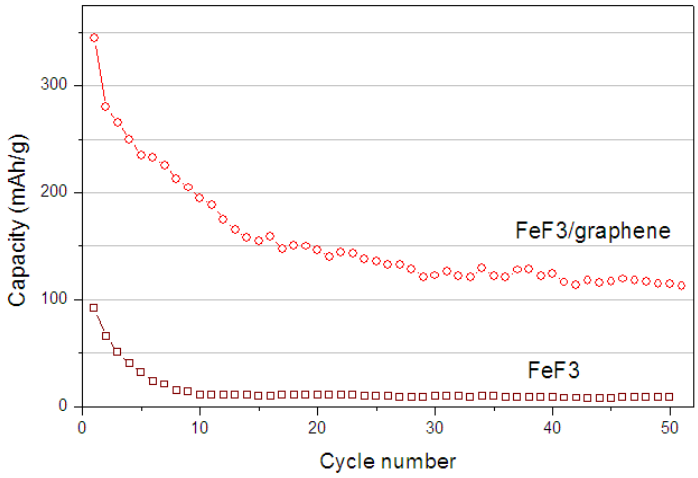

Fig. 4 the discharge curves of FeF_3 cathode and FeF_3/graphene cathode at 0.3 C at the range of 1.0-4.0 V for NIB.

4. Conclusions

In conclusion, the sheet-like structure FeF_3/graphene composite for the application of NIB was successfully synthesized by a facile sol-gel route. The sheet-structural formation between FeF_3 and graphene for FeF_3/graphene composite can contribute positively to the large reversible Na-storage capacity compared with FeF_3 during insertion/deinsertion process as well as conversion reaction. In the aspect of electrochemical behavior, FeF_3/graphene exhibits a fairly high initial discharge capacity of 550 mAh g^{-1} at 0.1 C, and it can still retain 115.8 mAh g^{-1} after 50 cycles at 0.3 C at a range of 1.0-4.0 V. Although the cycling performance and specific capacity of FeF_3/graphene need to be improved further, the design and preparation for the hybrid sheet-like structure FeF_3/graphene composite as the cathode material of

NIB is still a valuable exploration.

Acknowledgments

This work is supported financially by the National Natural Science Foundation of China under project No. 51472211, Scientific and Technical Achievement Transformation Fund of Hunan Province under project No. 2012CK1006, Key Project of Strategic New Industry of Hunan Province under project No. 2013GK4018, and Science and Technology plan Foundation of Hunan Province under project No. 2013FJ4062.

References

[1] S. W. Kim, D. H. Seo, X. Ma, G. Ceder, and K. Kang, Adv. Energy Mater., 2012, 2, 710–721.

[2] F. Sauvage, L. Laffont, J. M. Tarascon, and E. Baudrin, Inorg. Chem., 2007, 46 (8), 3289–3294.

[3] L. Zhao, J. Ni, H. Wang and L. Gao, RSC Adv., 2013, 3, 6650–6655.

[4] Y. Cao, L. Xiao, W. Wang, D. Choi, Z. Nie, J. Yu, L. V. Saraf, Z. Yang and J. Liu, Adv. Mater., 2011, 23, 3155–3160.

[5] M. D'Arienzo, R. Ruffo, R. Scotti, F. Morazzoni, C. M. Mari and S. Polizzi, Phys. Chem. Chem. Phys., 2012, 14, 5945–5952.

[6] M. Sathiya, K. Hemalatha, K. Ramesha, J. M. Tarascon, and A. S. Prakash, Chem. Mater., 2012, 24, 1846−1853.

[7] D. Kim, E. Lee, M. Slater, W. Lu, S. Rood, and C. S. Johnson, Electrochem. Commun., 2012, 18, 66–69.

[8] H. Yoshida, N. Yabuuchi, K. Kubota, I. Ikeuchi, A. Garsuch, M. S. Dobrick and S. Komaba, Chem. Commun., 2014, 50, 3677–3680.

[9] Y. H. Jung, C. H. Lim, J. H. Kim and D. K. Kim, RSC Adv., 2014, 4, 9799–9802.

[10] P. Barpanda, J. Lu, T. Ye, M. Kajiyama, S. Chung, N. Yabuuchi, S. Komaba and A. Yamada, RSC Adv., 2013, 3, 3857–3860.

[11] R. Tripathi, S. M. Wood, M. S. Islam and L. F. Nazar, Energy Environ. Sci., 2013, 6, 2257–2264.

[12] Z. Jian, L. Zhao, H. Pan, Y. S. Hu, H. Li, W. Chen, and L. Chen, Electrochem. Commun., 2014, 14, 86–89.

[13] K. T. Lee, T. N. Ramesh, F. Nan, G. Botton, and L. F. Nazar, Chem. Mater., 2011, 23, 3593–3600.

[14] M. Nishijima, I. D. Gocheva, S. Okada, T. Doi, J. Yamaki, T. Nishida, J. Power Sources, 2009, 190, 558–562.

[15]C. Li, C. Yin, L. Gu, R. E. Dinnebier, X. Mu, P. A. Aken , and J. Maier, J. Am. Chem. Soc., 2013, 135 (31), 11425–11428.

[16]C. Li, C. Yin, X. Mu, and J. Maier, Chem. Mater., 2013, 25 962−969.

[17] L. D. Carlo, D. E. Conte, E. Kemnitz and N. Pinna, Chem. Commun., 2014, 50, 460−462.

[18] Q. Chu, Z. Xing, X. Ren, A. M. Asiri, A. O. Al-Youbi, K. A. Alamry, X. Sun, Electrochim. Acta, 2013, 111, 80–85.

[19] L. Liu, H. Guo, M. Zhou, Q. Wei, Z. Yang, H. Shu, X. Yang, J. Tan, Z. Yan, and

X. Wang, J. Power Sources, 2013, 238, 501–515.

[20] J. Liu, Y. Wan, W. Liu, Z. Ma, S. Ji, J. Wang, Y. Zhou, P. Hodgson and Y. Li, J. Mater. Chem. A, 2013, 1, 1969–1975.

[21] Y. Yamada, T. Doi, I. Tanaka, S. Okada, and J. Yamaki, J. Power Sources, 2011, 196, 4837–4841.

[22] N. Dimov, A. Nishimura, K. Chihara, A. Kitajou, I. D. Gocheva, and S. Okada, Electrochim. Acta, 2013, 110, 214–220.

[23] L. Hu, Z. Tang, Z. Zhang, J. Power Sources, 2007, 166, 226–232.

[24] S. Han, L. Hu, Z. Liang, S. Wageh, A. A. Al-Ghamdi, Y. Chen, and X. Fang, Adv. Funct. Mater., 2014, 24, 5719–5727.

[25] K. Teinz, S. Wuttke, F. Börno, J. Eicher, and E. Kemnitz, J. Catal., 2011, 282, 175–182.

[26] D. Ma, H. Wang, Y. Li, D. Xu, S. Yuan, X. Huang, X. Zhang and Y. Zhang, Nano Energy, 2014, 10, 295–304.